

Resolving the geometrically necessary dislocation content in severely deformed aluminum by transmission Kikuchi diffraction

Naghdy, Soroosh; Verleysen, Patricia; Petrov, Roumen; Kestens, Leo

DOI

[10.1016/j.matchar.2018.04.013](https://doi.org/10.1016/j.matchar.2018.04.013)

Publication date

2018

Document Version

Final published version

Published in

Materials Characterization

Citation (APA)

Naghdy, S., Verleysen, P., Petrov, R., & Kestens, L. (2018). Resolving the geometrically necessary dislocation content in severely deformed aluminum by transmission Kikuchi diffraction. *Materials Characterization*, 140, 225-232. <https://doi.org/10.1016/j.matchar.2018.04.013>

Important note

To cite this publication, please use the final published version (if applicable). Please check the document version above.

Copyright

Other than for strictly personal use, it is not permitted to download, forward or distribute the text or part of it, without the consent of the author(s) and/or copyright holder(s), unless the work is under an open content license such as Creative Commons.

Takedown policy

Please contact us and provide details if you believe this document breaches copyrights. We will remove access to the work immediately and investigate your claim.



Resolving the geometrically necessary dislocation content in severely deformed aluminum by transmission Kikuchi diffraction

Soroosh Naghdy^{a,*}, Patricia Verleysen^{a,2}, Roumen Petrov^{a,b,3}, Leo Kestens^{a,b,2}

^a EEMMeCS Department, Research group Materials Science and Technology, Ghent University, Belgium

^b Department of Materials Science and Engineering, Delft University of Technology, The Netherlands

ARTICLE INFO

Keywords:

Aluminum
High pressure torsion (HPT)
Transmission Kikuchi diffraction (TKD)
Grain fragmentation
Geometrically necessary dislocations (GNDs)

ABSTRACT

In this paper, severe plastic deformation (SPD) is applied to commercially pure aluminum. Monotonic high pressure torsion (HPT) processing is employed at room temperature, and the microstructure of samples deformed up to an equivalent strain of 50 is investigated by electron backscatter diffraction (EBSD). The distribution pattern and the density of geometrically necessary dislocations (GNDs) are evaluated by examination of transmission Kikuchi diffraction (TKD) maps. Three different methodologies are utilized for assessment of the GND density. It was observed that two distinct stages of grain fragmentation and steady-state occur during processing. During the first stage, a severe grain refinement was observed as the average grain size decreased from $\sim 85 \mu\text{m}$ to $\sim 1 \mu\text{m}$ at an equivalent strain of 10. Quantification of the density of dislocations in both deformation regimes showed that, independent of the choice of model, the GND density is greater in the fragmentation stage than in the steady-state stage. This observation was linked with the prevalence of the continuous dynamic recrystallization (CDRX) phenomenon in each stage. Furthermore, a significant presence of GNDs in the steady-state stage was characterized. Formation of microstructure, grain refinement and saturation of grain size are discussed in the light of statistics of GNDs.

1. Introduction

In modern high pressure torsion (HPT), Bridgman's concept is utilized to deform a disk shaped sample by placing it between two anvils and employing torsional straining while a massive compressive load is applied [1]. This deformation technique is a continuous process, meaning that, unlike many other severe plastic deformation (SPD) processes, repetitive reinsertion of the sample is not required during processing [2]. Because of the high hydrostatic pressure, a practically unlimited magnitude of strain can be imposed in a single operation. In this way, bulk nano-structured and ultrafine-grained (UFG) metallic materials can be efficiently manufactured by heavy straining [3,4]. Consequently, the mechanisms driving microstructural evolution at elevated strains can be investigated.

Dependent on the level of deformation, two distinct stages of microstructural evolution can be distinguished in the HPT process: in the first stage significant grain fragmentation is taking place, whereas in the last stage the grain size saturates [5]. During the fragmentation

process of the grains, new grain boundaries with increasing misorientations appear. The presence of these boundaries is necessary since they accommodate the developing misorientation across neighboring crystallite volumes [6]. Such boundaries are called geometrically necessary boundaries (GNBs), and a different selection and number of activated slip systems is observed on either side of the boundary. Accordingly, their constituent dislocations are known by geometrically necessary dislocations (GNDs).

Apart from GNDs, statistically stored dislocations (SSDs) contribute to the total dislocation density. While the misorientation angles across GNBs are large with a wide spread, a mutual trapping of SSDs leads to the formation of ordinary cell boundaries, with a relatively small misorientation and a narrow spread [7]. The formation of misorientations is modelled for both kinds of boundaries emphasizing the process of separation of dislocations of opposite sign. It is shown that fluctuations in the density of mobile dislocations lead to the formation of ordinary cell boundaries, whereas, even in the absence of statistical fluctuations, an additional contribution arises from a different activity of the slip

* Corresponding author at: Department of Electrical Energy, Metals, Mechanical Constructions and Systems (EEMMeCS), UGent, Tech Lane Ghent Science Park, Campus A, Technologiepark 903, B-9052 Zwijnaarde, Belgium.

E-mail address: Soroosh.Naghdy@UGent.be (S. Naghdy).

¹ Country of origin = Iran.

² Country of origin = Belgium.

³ Country of origin = Bulgaria.

systems on either side of the GNBs [8].

Since a local deformation field appears within the vicinity of each and every individual dislocation, all single dislocations are geometrically necessary. However, once a network of dislocations is treated as a continuum, a clear trend is observed. At large length scales any net geometric effect that SSDs would have, is counterbalanced by nearby dislocations of opposite sign within the Burgers circuit. The presence of GNDs, however, is characterized by a net Burgers vector, resulting in the gradual increase of lattice curvature and the emergence of an orientation difference [9]. It is believed that wherever non-uniform plastic deformation occurs, the GND density increases, and these additional GNDs contribute to hardening by acting as obstacles to mobile dislocations [10]. Therefore, the GND density may elucidate the heterogeneity of the local strain tensor and its development as a function of imposed strain.

The residual elastic lattice distortion caused by dislocations can be gauged by orientation contrast microscopy [11]. Provided a material model is available that connects the local orientation gradients with the dislocation content, the GND density can be computed. This relationship may be determined by the compatibility assumption of the elastic and the plastic deformation, leading to the fundamental relation of the dislocation theory [12]:

$$\nabla \times \beta^e = -\nabla \times \beta^p = \alpha \quad (1)$$

whereby β^e , β^p and α are the elastic lattice distortion, the plastic lattice distortion and the Nye tensors, respectively. The Nye tensor operates on a plane normal to produce the net Burgers vector for a circuit on that plane, and is related to the dislocation content of individual slip systems by [13]:

$$\alpha = \sum_{t=1}^N \rho^t \mathbf{b}^t \otimes \mathbf{v}^t \quad (2)$$

whereby ρ^t , \mathbf{b}^t and \mathbf{v}^t are the dislocation density, Burgers vector and line vector of each dislocation system t , respectively. A dislocation system, here, is defined as a unique combination of Burgers vector and line vector for a pure edge or screw dislocation. Dependent on the number of resolved terms in the Nye tensor, the crystallographic symmetry and the type of material model, the GND content can be estimated.

Owing to the development of a refined microstructure, often with a high density of crystallographic defects, conventional techniques are less applicable to characterization of SPD processed metals. As opposed to the finest obtainable spatial resolution by EBSD, i.e. 20–50 nm [14], transmission electron microscopy (TEM) can reach a spatial resolution of 2–3 nm [15]. The higher spatial resolution of TEM and the higher angular resolution of Kikuchi diffraction patterns in EBSD are combined in a recently developed technique, called Transmission Kikuchi Diffraction (TKD) [16–18]. In TKD, a TEM foil is used as a specimen in a scanning electron microscope and the Kikuchi diffraction pattern generated by the forward scattered electrons transmitted from the bottom of the foil is used for the indexation of the crystal structure [16]. The spatial resolution of the TKD depends on sample thickness, the atomic number of the material and the energy of the incident electrons [19]. Therefore, for severely deformed metallic samples, an effective characterization tool is offered which provides a significantly better spatial resolution in comparison to conventional EBSD.

In this article, a commercially pure aluminum alloy is deformed by HPT. The deformed samples, up to an equivalent strain of 50, were characterized by EBSD. The number of grains contained in each EBSD scan varied from 10^3 to 10^6 at different strain amplitudes. In order to obtain a better understanding of the deformation mechanisms, TKD technique was utilized. While EBSD served for a global analysis, TKD was used for a local analysis. The GND density is quantified by examination of the TKD maps, on the basis of three different methodologies. Each model is first explained, and the formation of microstructure, the grain refinement and the saturation of grain size are further discussed.

2. Material and sample processing

An initially cold rolled sheet of commercially pure aluminum with 1.2 mm thickness was heat-treated at 500 °C for 30 s, resulting in the formation of a fully recrystallized microstructure with an average grain size of 85 μm . Disks with 15 mm diameter were extracted from the sheet and deformed by HPT processing at room temperature. The torsional straining was applied with a constant rotation speed of 1 rpm, while a nominal pressure of 2.5 GPa was maintained. Revolutions of 1/8, 1/4, 1/2, 1, 2 and 5 corresponding to equivalent strains of up to 50 were imposed. The deformed samples were stored in a freezer at -20 °C before microstructural investigation.

For the EBSD measurements, the finely polished disks were electro-polished by A2 Struers electrolyte, under a voltage of 48 V during 20 s at 22 °C. For TKD, the samples were first ground to a thickness of 150 μm and then 3 mm disks were punched out of the sample. The samples were further thinned using a twin-jet electro-chemical polisher in a solution of 1/3 nitric acid and 2/3 methanol, until a central hole appeared, according to well-established procedure for TEM foil preparation. The inner edge of the sample is transparent for the electrons, which corresponds to a thickness between 40 and 80 nm. An EDAX-TSL EBSD system attached to an FEI environmental scanning microscope (Quanta 450 with a field emission gun) was used for both the EBSD and TKD measurements. EBSD was performed at an accelerating voltage of 15 kV, at a working distance of 16 mm and a tilt angle of 70°, whereas the TKD was performed at an accelerating voltage of 30 kV, at a working distance of 6 mm under a tilt angle of -10° . A beam current of 2.3 nA corresponding to FEI spot size #5 (for the final aperture of 30 μm) was used for the EBSD measurement. These parameters allow acquisition of the diffraction patterns in a square scan grid mode with direct indexing, providing acquisition speeds between 50 and 120 patterns per second. The location of observation is on the top surface of the disks, at a constant radius of 3 mm from the center, which corresponds to equivalent strains of 1, 2, 5, 10, 20, and 50. EBSD and TKD measurements were performed with step sizes of 100 and 20 nm, respectively.

The EBSD and TKD data were analyzed with the commercial TSL-OIM data analysis software version 6.1. For TKD, a cleanup procedure of grain confidence index standardization with a grain tolerance angle of 1° was employed on data points. The EBSD data were additionally processed by a grain dilation correction. The number of grains contained in each EBSD scan varied from 10^3 to 10^6 , which is sufficient to ensure a statistically representative sample.

3. The GND density evolution: methodology and results

The GND content was assessed based on examination of the TKD maps, shown in Fig. 1. In these maps, boundaries with rotation angles between 2 and 5°, 5–15° and higher than 15° are indicated in red, white and black lines, respectively. A pixel to pixel criterion is used for calculation of misorientations, meaning that the difference between each pixel and its neighbors is gauged. The evolution of the fragmentation process during large plastic deformation can be clearly seen. The emergence of white lines as extensions of red lines, and black lines as extensions of white lines is an indication of gradual misorientation of low angle grain boundaries (LAGBs) to high angle grain boundaries (HAGBs). In the following sections, details of each utilized approach for the GND estimation are presented.

3.1. Lower bound approach

The residual elastic lattice distortion caused by dislocations could be measured by diffraction techniques, and subsequently be used to recover the dislocation content of the material. Eq. 1 provides the material model required for this correlation, leading to the estimation of the Nye tensor. The Nye tensor, however, has at most nine terms while

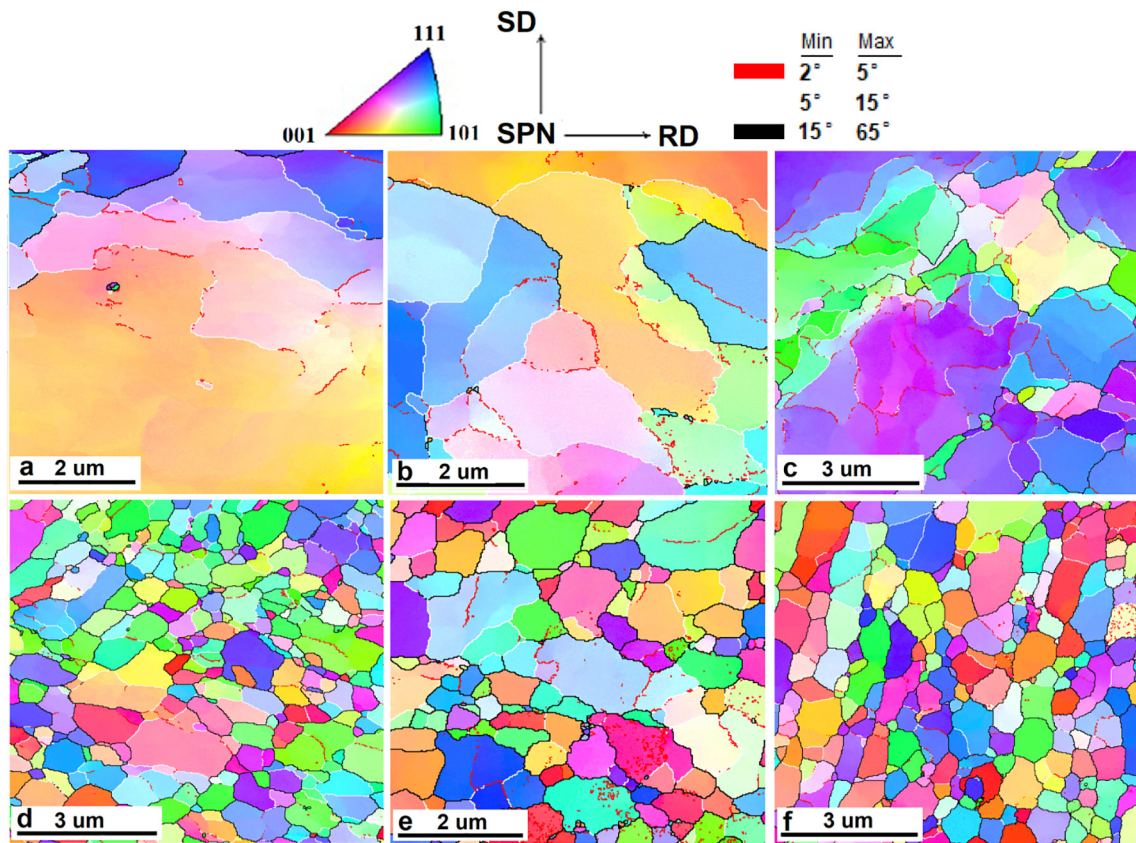


Fig. 1. Inverse pole-figure TKD maps depicting the grain structure at equivalent strains of a-1; b-2; c-5; d-10; e-20 and f-50. Individual grains are colored according to crystal direction coinciding with the shear plane normal (SPN) direction, c.f. attached color key. RD and SD stand for the radial and the shear directions, respectively. Boundaries with rotation angles between 2 and 5°, 5–15° and higher than 15° are indicated in red, white and black lines, respectively. (For interpretation of the references to color in this figure legend, the reader is referred to the web version of this article.)

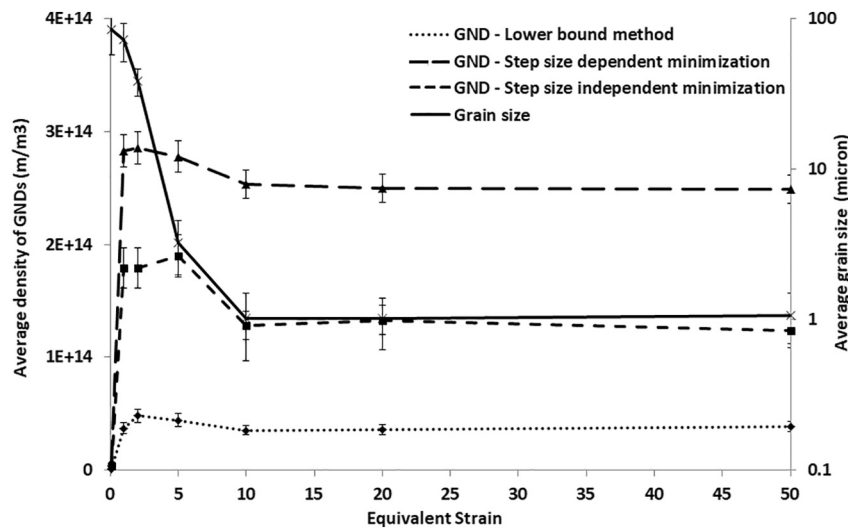


Fig. 2. Average density of GNDs calculated based on three different methodologies, together with the evolution of grain size as a function of imposed strain.

face centered cubic (FCC) materials have 18 dislocation systems [20]. Therefore, Eq. (2) is under-constrained when it is solved for the dislocation density of each individual dislocation system. It has been shown that for the case of simple cubic (SC) materials, for which there are only 9 orthogonal dislocation types, there is a one-to-one correspondence between the components of the Nye tensor and the dislocation densities, provided an appropriate reference frame is chosen. For more complex crystal systems, the SC deconstruction acts as an

approximate lower bound for the dislocation density. In a SC crystal structure, the GND density could be precisely determined by [12,13]:

$$\rho = \frac{1}{|b|} \|\alpha\|_1 \quad (3)$$

whereby $\|\alpha\|_1 = \sum_i \sum_j |\alpha_{ij}|$, is the entry-wise one-norm of the Nye tensor. Surface characterization techniques, however, resolve gradients of the Nye tensor in only two directions. Therefore, only three terms, representing the net Burgers vector for a circuit in the sample plane of

measurement, can be fully recovered. Two additional terms may be resolved, if unknown elastic strain components are neglected [13]. Hence, at best, 5 out of 9 components of the Nye tensor can be derived from two-dimensional mapping. From them, a truncated scalar value of ρ_{GND}^{2D} can be calculated, which represents the GND density in the plane of measurement. Assuming isotropic properties for the Nye tensor, the three dimensional density can be estimated by [21]:

$$\rho = \frac{1}{|\mathbf{b}|} \|\alpha\|_1 = \frac{1}{|\mathbf{b}|} \left(\sum_i \sum_j |\alpha_{ij}| \right) = \frac{3}{\sqrt{5}} \rho_{GND}^{2D} \quad (4)$$

The explained procedure is applied to the TKD maps. In order to have an accurate estimation of the GND density, it is important to exclude HAGBs from the examination. Therefore, only misorientations equal and smaller than 5° are considered for the three methods used in this paper. The estimated average density of GNDs is shown in Fig. 2. Next to the density obtained from the lower bound method, results of step-size dependent/independent minimization models, discussed in sections 3–2 and 3–3, respectively, are shown. A density number is reported at zero strain as well, calculated based on evaluation of the EBSD scan performed on annealed material. Additionally, the evolution of grain size at different strain amplitudes is shown.

The average GND density for annealed material is $9.6 \times 10^{11} \text{ m/m}^3$, increasing by a factor of nearly 50 at a strain of 1. A further growth to a maximum is observed at a strain of 2, followed by a decrease until a plateau is established at strains larger than 10. This strain might be considered as a transition from the fragmentation to the steady-state stage, since further significant grain refinement is not observed at higher strains. Deformation results in a decrease of the grain size from $85 \pm 22.50 \mu\text{m}$ to $1.01 \pm 0.42 \mu\text{m}$ at a strain of 10, followed by a minor alteration to $1.05 \pm 0.38 \mu\text{m}$ at a strain of 50.

3.2. Step size dependent minimization approach

For the FCC crystals, GNDs are either pure screw dislocations with line and Burgers vectors along $\langle 110 \rangle$ (6 types) or pure edge with $\langle 110 \rangle$ Burgers vectors and $\langle 1\bar{1}2 \rangle$ line directions (12 types) [20,22]. Dislocations of mixed character are considered as linear combinations of pure edge and screw systems. FCC crystals have 18 unique dislocation systems, but if derivatives are taken in 3 orthogonal directions, at most 9 constraints are provided by the Nye tensor, c.f. Eq. (2). Additional constraints, typically incorporated in some form of optimization approach, must be employed to find a reasonable estimate of the dislocation density.

One of the most common approaches involves minimizing the objective function $\sum_{i=1}^{18} (\rho^i)^2$, also known as L_2 -minimization method [12]. In this approach the L_2 norm of the individual dislocation densities is minimized, leading to the computation of the density of all 18 dislocation systems. The average density of GNDs and their distribution pattern are shown in Figs. 2 and 3, respectively.

The evolution trend is in agreement with the calculated density from the lower bound approach, but the estimated numbers are about one order of magnitude greater, c.f. Fig. 2. The distribution pattern represents a smaller concentration of GNDs in the center of grains and a larger accumulation in the vicinity of already existing HAGBs, c.f. Fig. 3.

3.3. Step size independent minimization approach

The step size of measurement, can affect the distinction between SSDs and GNDs, since this parameter defines the implicit Burgers vector. Theoretically, if the Burgers circuit size is smaller than the dislocation dipole size, all dislocations can be measured as GNDs [23]. Researchers have already shown that measured GND density is a function of the step size of the EBSD scan. It is reported that smaller step sizes lead to a greater GND density, whereas with increase of length scale, a so-called transformation of GNDs to SSDs takes place [24].

This size dependence can be investigated if the measurement is performed with a fine step size. To this purpose, the TKD maps with an initial step size of 20 nm were processed, and new maps were generated by successive elimination of data. Each time, the step size of measurement was increased by a factor of two, until the microstructural features completely disappeared at a step size of 1280 nm. The GND content of each map was calculated by the L_2 -minimization method, and the evolution of density as a function of step size was studied.

Fig. 4 illustrates an example of this approach, for a sample deformed up to an equivalent strain of 2. The GND curve is divided into three distinguished regions: two descending regions, inversely proportional to the step size of measurement, separated by a roughly constant zone. The occurrence of region A is attributed to some combination of algorithmic noise and the GND to SSD transition. At larger, moderate step sizes in region B, the measured GND density is roughly constant. It is suggested that this constant region is the result of true GNDs that accommodate strain gradients on the scale of the material substructure. Finally, in region C, the GND density drops off again. This decrease is only observed at very large step sizes, often larger than the grain size of the material.

This approach was applied to all deformed samples, and the step size corresponding with region B was determined to be between 80 and 320 nm. The calculated values lie between the GND contents assessed by the two previous methods, c.f. Fig. 2. The evolution trend reveals a relatively larger GND density in the fragmentation stage, the occurrence of a maximum at a strain of 5 and eventually saturation in the steady-state stage.

4. Discussion

Estimation of the GND density in both deformation regimes showed a relatively larger value in the fragmentation stage, followed by a decrease to a plateau in the saturation regime. In order to study the evolution of different boundary families, the boundary misorientation profiles are evaluated from EBSD measurements, c.f. Fig. 5.

In these profiles, the grain orientations with a cut-off angle of 5° are first averaged and the misorientation between adjacent grains is gauged. Therefore the results are independent of the step size of the scan, and can be compared with the Mackenzie distribution [25]. The latter gives the probability density of observing a particular disorientation angle between randomly oriented cubic crystals. Once the imposed strains are relatively smaller, a distinguished peak is recognized in the LAGB region. With straining, the peak translates from the LAGB region to the HAGB region, in agreement with TKD results, c.f. Fig. 1. The disappearance of the LAGB region at the expense of the HAGB region is, in fact, an indication of the grain fragmentation mechanism. Finally, at strains larger than 10, the misorientation profiles approach a random distribution with a slight alteration at different strain amplitudes.

In simple shear deformation, as opposed to other deformation modes, it is possible for orientations close to stable positions to rotate away from the stable orientation. This may affect the frequency of LAGB to HAGB transformation, and explain the burst of HAGBs in Fig. 5. The evolution of individual orientations was studied during HPT processing of aluminum at room temperature. An oscillatory texture was observed with a dynamic change of texture components at different strain levels [26]. This asymmetric convergent/divergent nature of the rotation field was used to simulate generation of new HAGBs in commercially pure aluminum during hot torsion [27]. This phenomenon was reported to encourage the fragmentation of mother grains and result in generation of additional HAGBs.

During HPT processing, grains tend to display an oblate shape in space, with a finite aspect ratio between the largest and the shortest axes of ellipsoids [5,28,29]. Comparison with the theoretical grain shape evolution provides interesting insights. Calculations, based on the geometry of simple shear deformation, predict extreme aspect ratios for

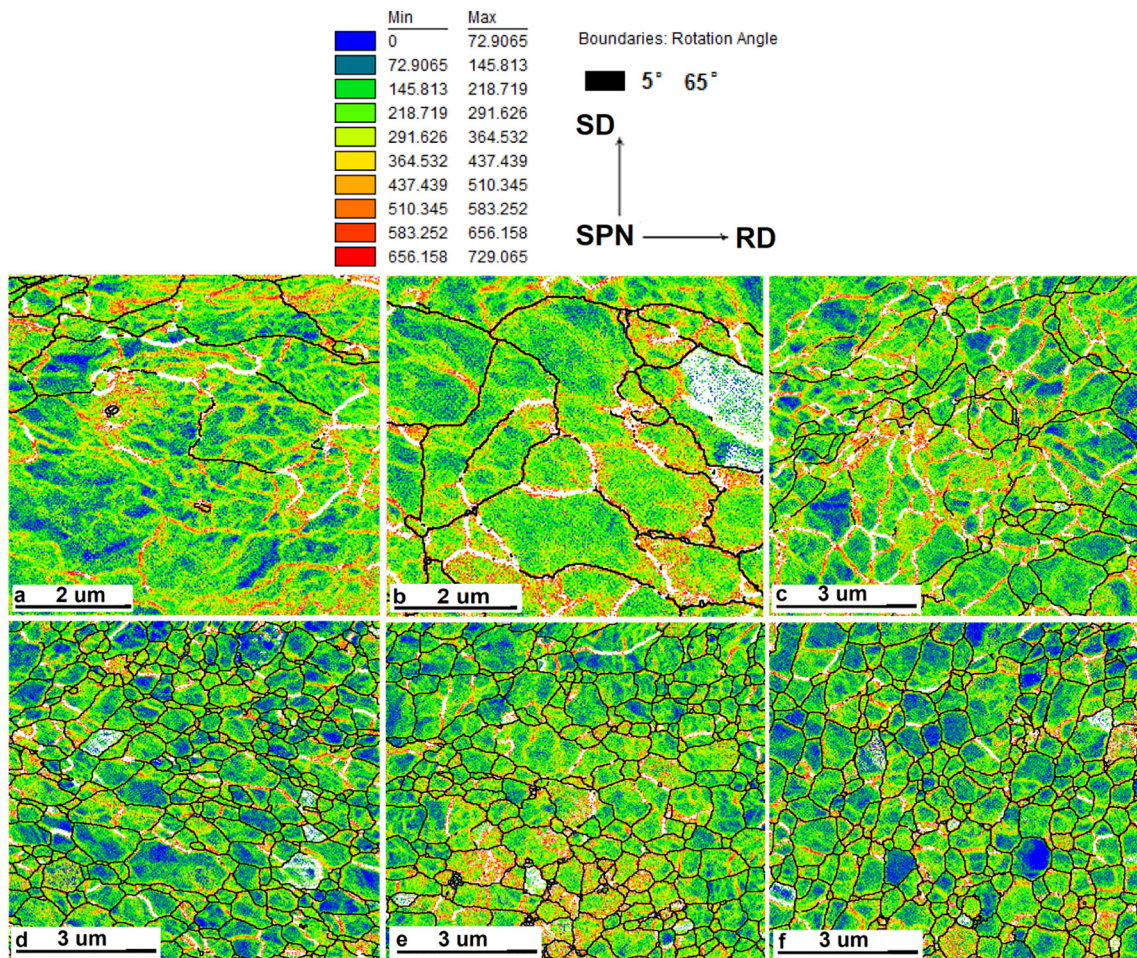


Fig. 3. The distribution pattern of GNDs (units are $\times 10^{12} \text{ m}^{-3}$) at equivalent strains of a-1; b-2; c-5; d-10; e-20 and f-50. Boundaries with a misorientation larger than 5° are shown with solid black lines. RD, SD and SPN stand for the radial, the shear, and the shear plane normal directions, respectively.

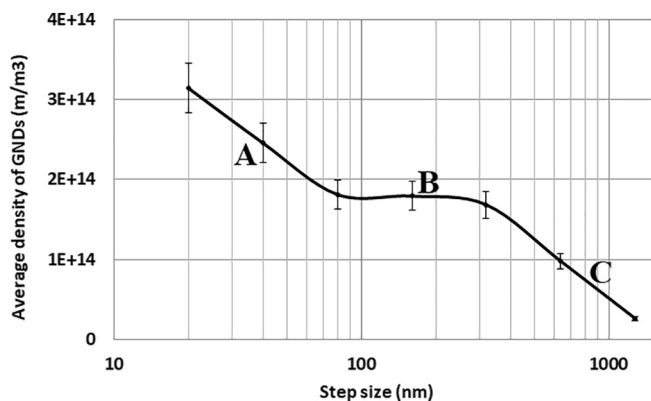


Fig. 4. The average GND density computed by the L_2 -minimization method as a function of the measurement step size, calculated for the deformed sample at a strain of 2.

large plastic strains [28]. This discrepancy is often explained by the occurrence of dynamic recrystallization (DRX) process [30]. Discontinuous DRX (DDRX) and continuous DRX (CDRX) are well documented in SPD processing of aluminum.

DDRX is the classical recrystallization mechanism in which nucleation is followed by growth, while CDRX operates by progressive accumulation of dislocations in subgrain boundaries, associated with a gradual increase of misorientation and formation of new grain boundaries [31,32]. The grain boundary migration rate controls the type of

DRX mechanism during deformation [33,34]. If the time needed for transformation of a subgrain boundary into a large angle grain boundary is significantly smaller than the time needed for a mobile grain boundary to sweep a distance equal to the microstructure size, the CDRX and the DDRX will be prevalent and negligible, respectively.

During the fragmentation stage, the refinement of grains follows a pattern of gradual increase of misorientation. The use of the Kernel average misorientation (KAM) map in combination with the image quality (IQ) map, visualizes this transformation. While all boundaries appear to have the same character in the IQ map, their different natures are clearly characterized in the KAM map, c.f. Fig. 6. Accumulation of dislocations results in the formation of GNBs, and HAGBs develop by gradual misorientation of boundaries with a lower rotation angle. This transformation, manifested in the intragranular microstructure which develops during straining, was studied by a recent grain refinement polycrystal model [35]. By modelling the gradual increase of lattice curvature within the mother orientation, the formation of GNBs was simulated. In agreement with findings of the current study, an initial increase of the GND density was predicted, followed by a decrease at larger strains. In our study, a significant presence of GNDs is characterized in both deformation regimes, suggesting that the DDRX mechanism is not pertinent to HPT processing of commercially pure aluminum. The collective arrangement of GNDs, however, resembles similarities with the features of the CDRX process, c.f. Figs. 3 and 6.

The lower-bound approach, explained in sections 3–1, was utilized to evaluate the GND density during SPD processing of commercially pure copper [36]. An increase of the GND content to a maximum at a strain of 2 was characterized, followed by a decrease until reaching the

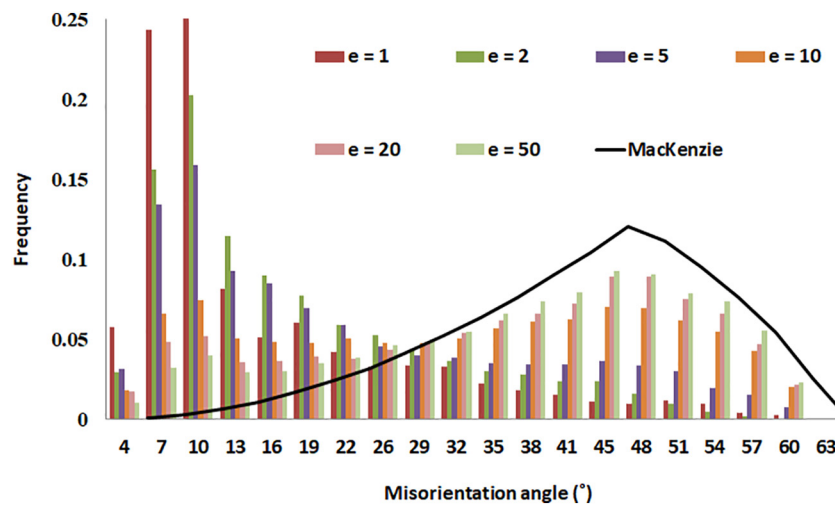


Fig. 5. The misorientation angle distribution calculated from EBSD data at different strain amplitudes (e), together with the theoretical Mackenzie distribution for an FCC polycrystal with a random distribution of grain orientations. The number of grains contained in each EBSD scan varies from 10^3 at $e = 1$ to 10^6 at $e = 50$.

stationary limiting stage of grain refinement at a strain of 14. The decrease of the GND density in the steady-state stage with respect to the maximum value in the fragmentation stage was about a factor of two. The higher GND density in the fragmentation stage was attributed to the higher rate of the CDRX occurrence. Additionally, the reduction of the GND density was reported to alleviate the heterogeneities of plastic deformation. In the saturation regime, a change towards a near homogenous Taylor type behavior of the polycrystal was determined [36].

In our study, the factor of decrease in the GND density is not as large as the SPD processing of pure copper. For example the ratio between the GND contents between the strain amplitudes of 20 and 2 are 0.75, 0.87 and 0.74 for the lower bound, step size dependent and step size independent approaches, respectively. Indeed, a relative decline of the GND content is indicative of the development of a more homogenous local strain tensor. Although the average grain size does not alter at extremely large strains, the GND contents remain comparable between two deformation stages. The continuous formation of the GNBs and yet the saturation of grain refinement, suggest that the effects of

fragmentation mechanisms are kept in balance by grain growth.

DDR, grain boundary sliding (GBS) and stress-induced grain boundary migration are amongst the proposed mechanisms leading to a possible grain growth during large plastic deformation. GBS is suggested as the deformation mechanism accounting for superplasticity, during which the generation of new defects is restricted [37]. The effective occurrence of GBS is often characterized with either a shift from the ideal positions of the deformation texture [38] or a massive randomization of texture [39]. Naghdy et al. [26] studied the texture evolution of commercially pure aluminum during HPT processing by means of large area EBSD scans. Neither a considerable shift nor a massive randomization was recognized in the saturation regime. In fact, it was observed that the weakening of the texture mostly occurs in the fragmentation stage. Minor alterations of texture intensity in the saturation stage were attributed to the constant rotation of every grain, resulting from the periodic convergence and divergence which take place in the vicinity of ideal positions.

The saturated grain shape was studied during monotonic HPT processing of Armco iron [40]. A temperature dependent behaviour was

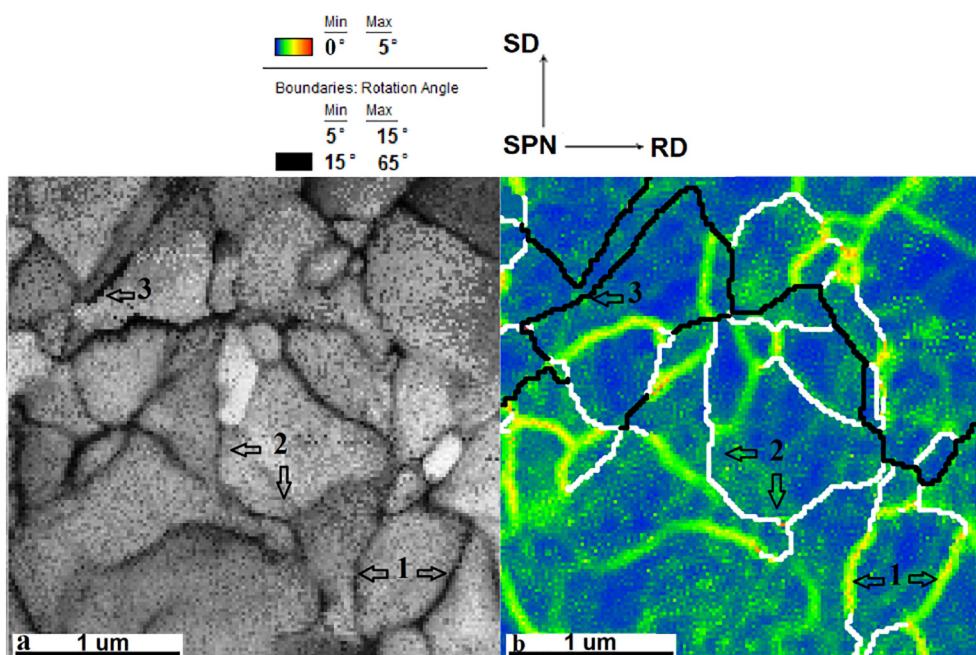


Fig. 6. a- image quality map and b- Kernel average misorientation map shown for the TKD measurement of a sample deformed up to an equivalent strain of 5. Boundaries with rotation angles between 5 and 15° and higher than 15° are indicated in white and black lines, respectively. RD, SD and SPN stand for the radial, the shear, and the shear plane normal directions, respectively.

characterized: the higher the temperature, the more equiaxed the microstructure. A diffusional grain boundary migration mechanism was characterized at high temperatures, whereas a preferential movement of atoms was detected at low temperatures. It was suggested that the migration of grain boundaries is governed by high-stresses in the latter, resulting in the occurrence of a directional microstructure [5,40].

Application of an external mechanical stress field together with internal sources, manifested in capillary forces arising from the small curvature of grain boundaries and accumulation of dislocations in pile-ups, may lead to the motion of grain boundaries. In situ tensile TEM experiments on a nano-crystalline high purity aluminum film at room temperature revealed two different types of stress-induced grain boundary migration: slow with an average growth speed of 0.2 nm s^{-1} and fast with an average speed of 50 nm s^{-1} [41]. The former was associated with a diffusion induced mechanism while the latter clearly represented features of a conservative, or non-diffusional, mechanism.

The morphological anisotropy that develops during simple shear deformation of aluminum was determined by three dimensional EBSD in [28]. It was reported that the grains exhibit an ellipsoidal shape in space with a favorable inclination in the saturation regime. An average angle of 20° was determined between the major axis of the ellipsoids and the shear direction. It was suggested that a stress induced grain growth phenomenon, with features of a conservative mechanism, leads to an increase of the average grain size in the saturation regime. Following that, the CDRX process takes place to refine the grain size. The occurrence of the stress-induced grain growth mechanism may explain the microstructural directionality, whereas its combination with the CDRX process can result in the saturation of grain refinement.

In reality, a combination of all above mentioned phenomena may be present in the saturation regime. Mechanisms leading to a major annihilation of dislocations, e.g. DDRX, may be less prevalent, as is suggested by the GND statistics in the current study. On the contrary, the incessant formation of GNBs implies that the CDRX mechanism is present in all strain amplitudes, with a higher frequency in the fragmentation stage. Sliding along microstructural boundaries is yet another possible phenomenon, during which the generation of dislocations is inhibited and therefore the GND content remains unchanged. Furthermore, stress induced grain boundary migration, either diffusional or conservative, may occur. A conservative occurrence of this mechanism, additionally, overcomes the difficulties of medium distance diffusion in the low temperature and explains the reported directionality of the microstructure.

5. Conclusions

The evolution of the microstructure in severely deformed aluminum was investigated by EBSD and TKD, and the GND density was estimated using three different approaches. Two distinct stages of grain fragmentation and steady-state were characterized, and a severe decrease of grain size from $\sim 85 \mu\text{m}$ to $\sim 1 \mu\text{m}$ was observed. Quantification of the GND density revealed a higher density in the fragmentation stage, independent of the approach used to quantify the GND. The process of refinement of grains followed a pattern of gradual increase of misorientation and transformation of LAGBs to HAGBs. This phenomenon was explained by the features of the CDRX mechanism. The higher GND content in the fragmentation stage was linked with the increased occurrence of the CDRX phenomenon.

A dynamic generation of GNBs was observed in the saturation regime. The ratio between the GND contents in the saturation and the fragmentation stages were 0.75, 0.87 and 0.74 for the lower bound, the step size dependent and the step size independent approaches, respectively. The occurrence of potential grain growth mechanisms, which can counterbalance the effects of the fragmentation mechanisms, was discussed. The GND statistics implied that the DDRX mechanism does not take place effectively. GBS is yet another deformation mechanism which can lead to a constant density of GNDs in the saturation regime.

A major occurrence of this phenomenon can lead to a massive randomization of texture, which is not in agreement with published results. A stress-induced grain boundary migration mechanism was found more in agreement with the statistics of GNDs. This mechanism may take place either diffusional or conservative. A diffusional mechanism is of a slow nature, whereas the occurrence of a conservative mechanism can also explain the reported directionality of microstructure.

Acknowledgements

The authors would like to acknowledge the Interuniversity Attraction Poles Program (IUAP) of the Federal Science Policy of Belgium and the partners of IUAP-VII-project P7/21 'Multiscale mechanics of interface dominated materials'.

Data availability

The raw/processed data required to reproduce these findings cannot be shared at this time as the data also forms part of an ongoing study.

References

- [1] A.P. Zhilyaev, T.G. Langdon, Using high-pressure torsion for metal processing: fundamentals and applications, *Prog. Mater. Sci.* 53 (2008) 893–979.
- [2] T.G. Langdon, Twenty-five years of ultrafine-grained materials: achieving exceptional properties through grain refinement, *Acta Mater.* 61 (2013) 7035–7059.
- [3] R.Z. Valiev, R.K. Islamgaliev, I.V. Alexandrov, Bulk nanostructured materials from severe plastic deformation, *Prog. Mater. Sci.* 45 (2000) 103–189.
- [4] Y.T. Zhu, X.Z. Liao, X.L. Wu, Deformation twinning in nanocrystalline materials, *Prog. Mater. Sci.* 57 (2012) 1–62.
- [5] R. Pippan, S. Scheriau, A. Taylor, M. Hafok, A. Hohenwarther, A. Bachmaier, Saturation of fragmentation during severe plastic deformation, *Annu. Rev. Mater. Res.* 40 (2010) 319–343.
- [6] N. Hansen, R.F. Mehl, A. Medalist, New discoveries in deformed metals, *Metall. Mater. Trans. A* 32 (2001) 2917–2935.
- [7] W. Pantleon, N. Hansen, Dislocation boundaries—the distribution function of disorientation angles, *Acta Mater.* 49 (2001) 1479–1493.
- [8] W. Pantleon, On the statistical origin of disorientations in dislocation structures, *Acta Mater.* 46 (1998) 451–456.
- [9] O. Rezvanian, M.A. Zikry, A.M. Rajendran, Statistically stored, geometrically necessary and grain boundary dislocation densities: microstructural representation and modelling, *Proc. R. Soc. Lond. Math. Phys. Eng. Sci.* 463 (2007) 2833–2853.
- [10] M.F. Ashby, The deformation of plastically non-homogeneous materials, *Philos. Mag.* 21 (1970) 399–424.
- [11] S.I. Wright, M.M. Nowell, D.P. Field, A review of strain analysis using electron backscatter diffraction, *Microsc. Microanal.* 17 (2011) 316–329.
- [12] D.P. Field, P.B. Trivedi, S.I. Wright, M. Kumar, Analysis of local orientation gradients in deformed single crystals, *Ultramicroscopy* 103 (2005) 33–39.
- [13] W. Pantleon, Resolving the geometrically necessary dislocation content by conventional electron backscattering diffraction, *Scr. Mater.* 58 (2008) 994–997.
- [14] S. Suzuki, Features of transmission EBSD and its application, *JOM* 65 (2013) 1254–1263.
- [15] P.W. Trimby, Orientation mapping of nanostructured materials using transmission Kikuchi diffraction in the scanning electron microscope, *Ultramicroscopy* 120 (2012) 16–24.
- [16] R.r. Keller, R.h. Geiss, Transmission EBSD from 10 nm domains in a scanning electron microscope, *J. Microsc.* 245 (2012) 245–251.
- [17] R. Geiss, R. Keller, S. Sitzman, P. Rice, New method of transmission Electron diffraction to characterize nanomaterials in the SEM, *Microsc. Microanal. Camb.* 17 (2011) 386–387.
- [18] R.H. Geiss, R.R. Keller, D.T. Read, Transmission electron diffraction from nanoparticles, nanowires and thin films in an SEM using conventional EBSD equipment, *Microsc. Microanal. Camb.* 16 (2010) 1742–1743.
- [19] K.p. Rice, R.r. Keller, M.p. Stoykovich, Specimen-thickness effects on transmission Kikuchi patterns in the scanning electron microscope, *J. Microsc.* 254 (2014) 129–136.
- [20] A. Arsenlis, D.M. Parks, R. Becker, V.V. Bulatov, On the evolution of crystallographic dislocation density in non-homogeneously deforming crystals, *J. Mech. Phys. Solids* 52 (2004) 1213–1246.
- [21] L.S. Toth, C. Gu, Ultrafine-grain metals by severe plastic deformation, *Mater. Charact.* 92 (2014) 1–14.
- [22] J. Jiang, T.B. Britton, A.J. Wilkinson, Accumulation of geometrically necessary dislocations near grain boundaries in deformed copper, *Philos. Mag. Lett.* 92 (2012) 580–588.
- [23] T.J. Ruggles, D.T. Fullwood, Estimations of bulk geometrically necessary dislocation density using high resolution EBSD, *Ultramicroscopy* 133 (2013) 8–15.
- [24] J. Jiang, T.B. Britton, A.J. Wilkinson, Measurement of geometrically necessary dislocation density with high resolution electron backscatter diffraction: effects of detector binning and step size, *Ultramicroscopy* 125 (2013) 1–9.

- [25] J.K. Mackenzie, Second paper on statistics associated with the random disorientation of cubes, *Biometrika* 45 (1958) 229–240.
- [26] S. Naghdy, L. Kestens, S. Hertelé, P. Verleysen, Evolution of microstructure and texture in commercial pure aluminum subjected to high pressure torsion processing, *Mater. Charact.* 120 (2016) 285–294.
- [27] M.R. Barnett, F. Montheillet, The generation of new high-angle boundaries in aluminium during hot torsion, *Acta Mater.* 50 (2002) 2285–2296.
- [28] S. Naghdy, H. Pirgazi, P. Verleysen, R. Petrov, L. Kestens, Morphological and crystallographic anisotropy of severely deformed commercially pure aluminium by three-dimensional electron backscatter diffraction, *J. Appl. Crystallogr.* 50 (2017) 1512–1523.
- [29] T. Hebesberger, H.P. Stüwe, A. Vorhauer, F. Wetscher, R. Pippan, Structure of Cu deformed by high pressure torsion, *Acta Mater.* 53 (2005) 393–402.
- [30] W. Skrotzki, N. Scheerbaum, C.-G. Oertel, R. Arruffat-Massion, S. Suwas, L.S. Tóth, Microstructure and texture gradient in copper deformed by equal channel angular pressing, *Acta Mater.* 55 (2007) 2013–2024.
- [31] C. Chovet, S. Gourdet, F. Montheillet, Modelling the transition from discontinuous to continuous dynamic recrystallization with decreasing purity in aluminium, *Mater. Trans. JIM* 41 (2000) 109–112.
- [32] S. Gourdet, F. Montheillet, A model of continuous dynamic recrystallization, *Acta Mater.* 51 (2003) 2685–2699.
- [33] S. Gourdet, F. Montheillet, Effects of dynamic grain boundary migration during the hot compression of high stacking fault energy metals, *Acta Mater.* 50 (2002) 2801–2812.
- [34] F. Montheillet, J. Le Coze, Influence of purity on the dynamic recrystallization of metals and alloys, *Phys. Status Solidi A* 189 (2002) 51–58.
- [35] L.S. Tóth, Y. Estrin, R. Lapovok, C. Gu, A model of grain fragmentation based on lattice curvature, *Acta Mater.* 58 (2010) 1782–1794.
- [36] L.S. Toth, C.F. Gu, B. Beausir, J.J. Fundenberger, M. Hoffman, Geometrically necessary dislocations favor the Taylor uniform deformation mode in ultra-fine-grained polycrystals, *Acta Mater.* 117 (2016) 35–42.
- [37] N.Q. Chinh, P. Szommer, T. Csanadi, T.G. Langdon, Flow processes at low temperatures in ultrafine-grained aluminum, *Mater. Sci. Eng. -Struct. Mater. Prop. Microstruct. Process.* 434 (2006) 326–334.
- [38] W. Skrotzki, A. Eschke, B. Jóni, T. Ungár, L.S. Tóth, Y. Ivanisenko, L. Kurmanaeva, New experimental insight into the mechanisms of nanoplasticity, *Acta Mater.* 61 (2013) 7271–7284.
- [39] Y. Ivanisenko, W. Skrotzki, R. Chulist, T. Lippmann, K. Yang, L. Kurmanaeva, H.-J. Fecht, Information on deformation mechanisms in nanocrystalline Pd–10% Au inferred from texture analysis, *J. Mater. Sci.* 45 (2010) 4571–4577.
- [40] R.Z. Valiev, Y.V. Ivanisenko, E.F. Rauch, B. Baudelet, Structure and deformation behaviour of Armco iron subjected to severe plastic deformation, *Acta Mater.* 44 (1996) 4705–4712.
- [41] M. Legros, D.S. Gianola, K.J. Hemker, In situ TEM observations of fast grain-boundary motion in stressed nanocrystalline aluminum films, *Acta Mater.* 56 (2008) 3380–3393.